Energy and Power Engineering, 2014, 6, 54-68
Published Online April 2014 in SciRes. http://www.scirp.org/journal/epe
http://dx.doi.org/10.4236/epe.2014.64007

Scientific Research

Magnetic Field Enhancement in Ammonia-Water Absorption Refrigeration Systems

Moradeyo K. Odunfa[1*], Richard O. Fagbenle[2], Olanrewaju M. Oyewola[1], Olayinka S. Ohunakin[3]

[1]Mechanical Engineering Department, University of Ibadan, Ibadan, Nigeria
[2]Mechanical Engineering Department, Obafemi Awolowo University, Ile-Ife, Nigeria
[3]Mechanical Engineering Department, Covenant University, Ota, Nigeria
Email: [*]m.odunfa@mail.ui.edu.ng

Received 8 January 2014; revised 8 February 2014; accepted 15 February 2014

Abstract

Absorption enhancement has been considered as an effective way of improving coefficient of performance (COP) of refrigeration systems and magnetic enhancement is one of these methods. A model of magnetic field enhancement in ammonia-water absorption systems is presented in this paper. A numerical model using finite difference scheme was developed based on the conservation equations and mass transport relationship. Macroscopic magnetic field force was introduced in the momentum equation. The model was validated using data obtained from the literature. Changes in the physical properties of ammonia solution while absorbing both in the direction of falling film and across its thickness were investigated. The magnetic field was found to have some positive effect on the ammonia-water falling film absorption. The results indicate that absorption performance enhancement increased with magnetic intensity. The COP of simple ammonia solution absorption refrigeration system increased by 1.9% and 3.6% for magnetic induction of 1.4 and 3.0 Tesla respectively.

Keywords

Ammonia-Water Absorption Refrigeration, Magnetic Field Force, Ammonia Solution Concentration, Coefficient of Performance, Finite Difference Scheme, Numerical Solution

1. Introduction

Energy is vital for human sustainance on earth; modern energy for industrial development is largely based on

[*]Corresponding author.

How to cite this paper: Odunfa, M.K., Fagbenle, R.O., Oyewola, O.M. and Ohunakin, O.S. (2014) Magnetic Field Enhancement in Ammonia-Water Absorption Refrigeration Systems. *Energy and Power Engineering*, **6**, 54-68.
http://dx.doi.org/10.4236/epe.2014.64007

fossil fuels which if coupled with other human activities, have been unequivocally shown to be responsible for the warming of the climate system [1]-[3]. According to the United Nations Framework Convention on Climate Change (UNFCCC), global increases in CO_2 concentrations are due primarily to fossil fuel consumption together with land-use change (LUC) which provides another significant contribution [4]. Urgent actions are now being taken worldwide to stem the rising levels of greenhouse gases (GHGs) through mitigation and adaptation activities.

Activities involving mitigation include reduction in the use of fossil fuels through energy efficiency measures (both on the supply and the demand side) and the uptake of renewable and clean energy technologies; the drive for both renewable and clean energy technologies has similarly impacted on developments within the cooling technology sector. Cooling technologies basically may be divided into two categories viz: vapour compression and sorption systems. Sorption system is further sub-divided into absorption and adsorption systems. Vapour compression systems involve the use of mechanical device, such as a compressor for the compression process. In an absorption system the mechanical compression is replaced with a thermo-chemical fluid lifting process in the two fluids; mixture of a gas in a liquid has a strong affinity to form a solution. In the adsorption process a gas or liquid solute accumulates on the surface of a solid or more rarely, a liquid (adsorbent), forming a molecular or atomic film (the adsorbate). In the manufacturing of cooling machine/system, this global demand for efficient use of energy at minimum environmental cost has increased preference for absorption refrigeration systems driven by waste heat or solar thermal energy over the conventional mechanical compression systems powered by grid electrical energy. The general usual imbalance of energy demand and supply coupled with the environmental degradation and climate change impact in many developing countries/least developed economies has further increased the urgent need for use of high efficiency and sustainable energy technologies.

In the absorption process, heat and mass transfer usually take place within a thin liquid falling-film; this has received the attention of many researchers over the years especially in the last two decades as a result of its wider application in many modern devices, such as absorption air-conditioners, absorption chillers, absorption heat pumps etc. [5]. An aspect of absorption refrigeration is the absorption enhancement which is an effective way to improve the performance of absorption refrigeration systems. Three kinds of absorption enhancement exist [6]. The first method falls under the category of mechanical methods which improve the performance by modifying the shape, surface and structure of the heat transfer tubes [7]. The second type comprises of chemical methods which involve the addition of surfactant in the absorbent while the third kind is the addition of nano-particles in the absorbing solution e.g. addition of Cu, CuO and Al_2O_3 nano-particles into ammonia-water solution [6] and also Fe and Carbon nano-tubes (CNT) in lithium bromide-water solution [8]. Researches on nano-fluids/nano-particles in absorbent are categorized into five groups viz: (i) stability analysis and experiments (ii) property measurement such as thermal conductivity and viscosity (iii) convective and boiling heat transfer (iv) mass transfer in binary nanofluids and (v) theoretical analysis and model development.

However, the effect of magnetic field on absorption refrigeration system is seldomly mentioned in literatures despite its established influence on the absorption process of ammonia vapour into ammonia-water solution absorption refrigeration system [9]. The magnetic field may therefore also have certain influence on the absorption process in other absorption refrigeration systems such as water vapour into lithium bromide-water solution absorption system. Wen-Long *et al*. [10] investigated experimentally the effect of additive on falling film absorption of water vapour in aqueous LiBr in enhanced absorption process study. The experimental results showed that small amounts of additive can enhance the heat transfer of absorption process significantly and the enhancement degree is influenced by additive concentration and Reynolds number. Based on a dimensionless analysis of the Navier-Stokes equations applied to the falling film absorption process, a new dimensionless parameter known as surface renewal number (Rn) was introduced, and a semi-empirical equation of enhancement factor of additive was obtained. This shows that the enhancement effect of additive on Nusset number of absorption process is determined by the absorption's Marangoni number (Ma), the surface Marangoni number (MaA), the surface renewal number (Rn), the adsorption number (η), and the Reynolds number (Re). It was proved that the semi-empirical equation can agree satisfactorily with the experimental results by introducing the parameters related to surface tension into the equation. The study concluded as follows: (i) there is an optimum additive concentration in which the enhancement effect of additive is strongest, (ii) Ma, MaA, and Rn enlarge the enhancement of the heat transfer during absorption, (iii) the adsorption number η reduces the heat transfer of absorption, and (iv) the enhancement factor decreases as the Reynolds number increases. Furthermore, an experimental study by Yong *et al*. [8] also obtained the following results viz: (i) the vapour absorption rate increases

with increasing solution mass flow rate and the concentration of Fe nanoparticles and CNT; the effect of coolant mass flow rate on the vapour absorption rate is not significant under the experimental conditions, (ii) the heat transfer rate increases with rise in the solution mass flow rate while it is not much affected by the concentration of nanoparticles, (iii) the mass transfer enhancement is much more significant than the heat transfer enhancement in the binary nanofluids with Fe nanoparticles and CNT, and (iv) the mass transfer enhancement from the CNT (average 2.16 for 0.01 wt % and average 2.48 for 0.1 wt %) becomes higher than that from the Fe nanoparticles (average 1.71 for 0.01 wt % and average 1.90 for 0.1 wt %). It was therefore concluded that the CNT is a better candidate than Fe nanoparticles for performance enhancement in H_2O/LiBr absorption system.

An experimental investigation into the effect of external magnetic field on falling film absorption in an ammonia-water system was conducted by Xiao *et al*. [11]. The study established the following findings: (i) external magnetic field with the same direction as falling film has enhancing effect on absorption of ammonia-water, and the absorption enhancement is more obvious in stronger magnetic field, (ii) not all magnetic fields can enhance the ammonia-water absorption process. While the external magnetic field against the direction of falling film is exerted, the absorption variables in magnetic field are all smaller than those in conventional absorption without magnetic field exerted; the magnetic field with direction against falling film weakens the absorption of ammonia-water, (iii) the absorption can be more intense if the external magnetic field is combined with optimal operating conditions. Their results further show that the changes in the outlet cooling water temperature, absorption heat and absorption mass with and without external magnetic field exerted, are larger when the inlet solution concentration is lower.

In the area of numerical modeling of enhanced absorption system, the mathematical model for magnetic field enhanced absorption process for ammonia-water solution on a falling-film was established by Xiao *et al*. [11]. The changes in physical properties of ammonia-water solution in absorption, the variation of falling film and the convection in the direction of thickness of liquid film were all considered in the model. The effect of the magnetic field on the distribution of some parameters in falling-film absorption such as velocity, temperature and concentration and so on was all obtained. The numerical results obtained showed that magnetic field can improve the performance of ammonia-water falling-film absorption, and that the absorption strengthening effect increases with the enhancement increasing magnetic induction intensity. The strengthening effect was limited within the magnetic field intensity range of 0 to 3 Tesla; however, the strengthening effect was observed to be stronger in high intensity magnetic fields. For both un-enhanced and enhanced absorption cooling systems, several working fluids have been investigated among which are Lithium-bromide-water (LiBr-H_2O), Lithium-Chloride-water (LiCl-H_2O) and Ammonia-water (NH_3-H_2O). Moreover, all these are popularly used in single-stage and advanced absorption air-conditioning/heat pump technology.

In engineering problems, either probabilistic or deterministic methods could be used depending on the degree of accuracy required of the solution while validation could be carried out using experimental data or exact analytic solutions where such exist. Absorption process enhancement under a magnetic field has been established in Xiao *et al*. [11] as having an effect on falling-film Ammonia-Water absorption, but not on a smooth thin-liquid falling-film. This work therefore employs the finite difference method to establish velocity, temperature and concentration distributions in magnetic field enhanced absorption process on a smooth thin-liquid falling-film using ammonia-water refrigerant/absorbent combination. The results have been compared with those obtained by Xiao *et al*. [11] in the falling-film. Such an investigation would reveal sections of the absorber that might need to be redesigned and its material re-specified for optimal efficiency of refrigerant absorption by the absorbent. The smooth thin-liquid falling-film is different from non-smooth in the sense that the film-thickness in the smooth is defined and non wavy, whereas, non-smooth is usually complex to analyze in order to obtain complete and reliable results.

2. Mathematical Model

2.1. Assumptions

In developing the governing equations for this flow modeling of the absorption process in a smooth thin-liquid film, the following assumptions are made:

i. The flow is a fully developed steady laminar flow as shown in **Figure 1**, hence velocity (v) in Y-direction is zero.

ii. The fluid properties are constant and not varying with temperature and concentration.

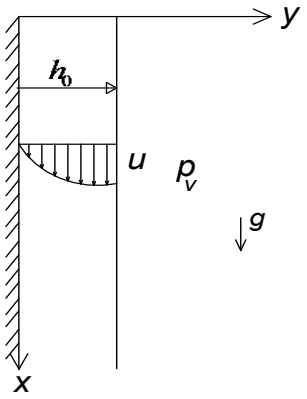

Figure 1. 2-d representation of a thin-liquid falling-film.

iii. The mass rate of vapour absorbed is very small compared to the solution flow rate such that the film thickness and flow velocities can be treated as constant.

iv. Heat transfer in the vapor phase is negligible.

v. Vapor pressure equilibrium exists between the vapour and liquid at the interface.

vi. The Peclet numbers are large enough such that the diffusion in the flow direction can be neglected.

vii. Diffusion thermal effects are negligible.

viii. The magnetic induction intensity decreases linearly along the flow of falling-film.

ix. The shear stress at the liquid-vapor interface is negligible.

Figure 1 is a schematic of the falling thin film wherein the x-axis is along the falling direction, and the y-axis is along the falling-film thickness direction. The velocity component in X and Y axis are u and v respectively. Heat transfer is described as the following energy equation:

$$\rho C_p u \frac{\partial T}{\partial x} + \rho C_p v \frac{\partial T}{\partial y} = \frac{\partial}{\partial y}\left(\lambda \frac{\partial T}{\partial y}\right) \tag{1}$$

In a similar way, the continuity equation, transport equation [12] and mass equation can be described as follows:

$$\frac{\partial(\rho u)}{\partial x} + \frac{\partial(\rho v)}{\partial y} = 0 \tag{2}$$

$$\frac{\partial^2 u}{\partial y^2} + 3\frac{v_0}{h^2_0} + \rho g + \int_{mag} = 0 \tag{3}$$

$$\rho u \frac{\partial \xi}{\partial x} + \rho v \frac{\partial \xi}{\partial y} = \frac{\partial}{\partial y}\left(\rho D_m \frac{\partial \xi}{\partial y}\right) \tag{4}$$

where $\int_{mag}$ Li [13] in the above equation is the magnetic force which the falling-film solution experienced per unit volume. The direction of which is vertically downward.

$$\int_{mag} = \frac{\rho \chi^{B^2}}{l \cdot \mu_0} \tag{5}$$

where χ is the magnetic mass susceptibility of either LiBr and or LiCl water solution, B is the magnetic induction intensity, l is the length of falling-film flows, and μ_0 is the vacuum's permeability, u is the velocity in the film in X-direction and

$$V_0 = \frac{\rho g h_0^2}{3\mu} \quad \text{or} \quad h_0 = \left(\frac{3\mu V_0}{\rho g}\right)^{\frac{1}{2}}$$

From the above-mentioned assumptions, the final model set of magnetic enhanced transport, heat and mass transfer equations on a smooth thin-liquid falling-film corresponding to the coordinate system shown in **Figure 1** will now be:

$$u\frac{\partial T}{\partial x}-\alpha\frac{\partial^2 T}{\partial y^2}=0 \tag{6}$$

$$\partial\frac{(\rho u)}{\partial x}=0 \tag{7}$$

$$\frac{\partial^2 u}{\partial y^2}+3\frac{v_0}{h^2{}_0}+\rho g+\frac{\rho\chi B^2}{l\mu_0}=0 \tag{8}$$

$$u\frac{\partial\xi}{\partial x}-D_m\frac{\partial^2\xi}{\partial y^2}=0 \tag{9}$$

The final model magnetic enhanced velocity field, heat and mass transfer equations on a smooth thin-liquid falling-film in a cooling system are:

$$\frac{\partial^2 u}{\partial y^2}+3\frac{v_0}{h^2{}_0}+\rho g+\frac{\rho\chi B^2}{l\mu_0}=0 \tag{10}$$

$$u\frac{\partial T}{\partial x}-\alpha\frac{\partial^2 T}{\partial y^2}=0 \tag{11}$$

$$u\frac{\partial\xi}{\partial x}-D_m\frac{\partial^2\xi}{\partial y^2}=0 \tag{12}$$

where χ is the magnetic mass susceptibility, B is the magnetic induction intensity, l is the length of falling-film flows, μ_0 is the vacuum permeability, T is temperature, ξ is concentration (absorbent), α is thermal diffusivity, D or D_m is species diffusivity, V_0 is the average velocity within the film thickness and h_0 is the film thickness

2.2. Boundary Conditions

$$\text{At } x = 0;\ u = u_{in},\ T = T_{in} \text{ and } \xi = \xi_{equil} \tag{13}$$

At y = 0; (non permeable wall);

$$u = 0,\ T = T_w,\ \frac{\partial\xi}{\partial y}=0 \tag{14}$$

$$\text{At } y = h_0;\ -K\frac{\partial T}{\partial y}=\rho D_m\frac{\partial\xi}{\partial y}H_a \tag{15}$$

$$\xi = \xi_{equil}\ (T,\ P_v) \tag{16}$$

At the vapour-liquid interface,

$$y = h_0;\ \left(\frac{\partial u}{\partial y}\right)_{y=0}=0, P_v=(T_s,\xi_s)=const.$$

where H_a = Heat of absorption, T_w = Wall temperature, P_v = Vapour pressure and $\xi_{equil}(T,P_v)$ = equilibrium concentration at the interface temperature and ambient vapour pressure.

3. Solution of the Model Equations

The continuity, momentum, energy and species mass transport equations presented earlier were coded in a computer algorithm using FORTRAN programming language. The solution technique used is Gaussian elimination

scheme as modified by Paynes and Iron on the digital computer. The computer program is written in FORTRAN 90 language. The code program and its subroutines description is as shown in the Appendix.

3.1. Computer Code

The computer code solves Equations (10)-(12) using modified Gaussian elimination scheme. The code was run on a personal computer with sufficient memory facilities to carry out the simulation exercise. The parameters utilized in the literature as shown in **Table 1** [11] [14] have also been used. In this present work, the domain area was divided into 13 × 5 mesh evenly spaced in both the direction of falling 1 m (×) and in the direction of film thickness 10^{-3} m (y). The grid size is 0.08 × 0.00025 m. While the result's pattern is grid-independent, the quality of the result to an extent is grid-dependent.

3.2. Data Employed

The data utilized from the literature are as shown in **Table 1**.

4. Results and Discussion

The results for velocity, temperature and concentration both in the direction of falling film and across its thickness were presented.

4.1. Results in the Direction of Falling-Film

The distribution of the significant parameters obtained in the direction of the falling film for Ammonia-water (NH_3-H_2O) solution agrees quite well with existing literature results. **Tables 2-4** shows the T-Test analysis results of the present data and the literature. It should be noted that the Test established that the velocity, temperature and concentration distributions for ammonia-water was not significantly different ($p > 0.05$) which show the agreement of the present data with the literature.

Figures 2-3 show the average velocity distributions of NH_3-H_2O in the film at 0.0, 1.4 and 3.0 Tesla. With reference to zero Tesla, there is a considerable change in the profile; the effect increases as the magnetic intensity increases. It was observed that the profile follows similar pattern as those of Xiao *et al*. [11]; it is thus suggested that magnetic flux stabilize the field which enhances the change in the average velocity. It should be noted that the changes are mild especially at the interface. This is not surprising since there is exchange of ac-

Table 1. NH_3-H_2O data.

Parameters	Values
film dynamic viscosity (μ)	4×10^{-4} kgm^{-1}·s^{-1}
vacuum Permeability (μ_0)	1.257×10^{-6} kgm·A^{-2}·s^{2}
Initial velocity (u_{in})	0.362 m·s^{-1}
Liquid density (ρ)	127 kg·m^{-3}
Thermal conductivity (K)	176 W·m^{-1}·K^{-1}
Wall Temperature (T_w)	35˚C
Inlet Temperature (T_{in})	35˚C
Initial absorbent Concentration (C_{in})	20%
Equilibrium absorb Conentration (C_{eq})	20%
Mean film thickness (h_o)	1.00×10^{-3} m
Absorbent Vapour Pressure (P_v)	7.02 mm·Hg
Film mass flowrate (I)	0.01 kg·m^{-1}·s^{-1}

Source: Xiao *et al*. [11].

Table 2. NH_3-H_2O velocity T-test analysis—independent samples test.

		Levene's Test for Equality of Variances		t-test For Equality of Means						
		F	Sig	t	df	Sig (2-tailed)	Mean Difference	Std. Error Difference	95% Confidence Interval of the Difference	
									Lower	Upper
Velocity @ 0.0 Tesla	Equal variances Assumed	0.023	0.881	0.234	24	0.817	0.001292	0.005526	−0.010114	0.012698
	Equal variances not assumed			0.234	23.992	0.817	0.001292	0.005526	−0.010114	0.012698
Velocity @ 1.4 Tesla	Equal variances Assumed	0.084	0.775	0.382	24	0.706	0.002192	0.005745	−0.009665	0.014050
	Equal variances not assumed			0.382	23.942	0.706	0.002192	0.005745	−0.009667	0.014051
Velocity @ 3.0 Tesla	Equal variances Assumed	0.018	0.893	0.507	24	0.617	0.002908	0.005740	−0.008939	0.14754
	Equal variances not assumed			0.507	23.961	0.617	0.002908	0.005740	−0.008940	0.014755

Table 3. NH_3-H_2O temperature T-test analysis—independent samples test.

		Levene's Test for Equality of Variances		t-test For Equality of Means						
		F	Sig	t	df	Sig (2-tailed)	Mean Difference	Std. Error Difference	95% Confidence Interval of the Difference	
									Lower	Upper
Velocity @ 0.0 Tesla	Equal variances Assumed	0.029	0.865	0.031	24	0.975	0.077	2.479	−5.039	5.193
	Equal variances not assumed			0.031	23.980	0.975	0.077	2.479	−5.039	5.193
Velocity @ 1.4 Tesla	Equal variances Assumed	0.029	0.865	0.031	24	0.975	0.077	2.479	−5.039	5.193
	Equal variances not assumed			0.031	23.980	0.975	0.077	2.479	−5.039	5.193
Velocity @ 3.0 Tesla	Equal variances Assumed	0.029	0.865	0.031	24	0.975	0.077	2.479	−5.039	5.193
	Equal variances not assumed			0.031	23.980	0.975	0.077	2.479	−5.039	5.193

Table 4. NH_3-H_2O concentration T-test analysis—independent samples test.

		Levene's Test for Equality of Variances		t-test For Equality of Means						
		F	Sig	t	df	Sig (2-tailed)	Mean Difference	Std. Error Difference	95% Confidence Interval of the Difference	
									Lower	Upper
Velocity @ 0.0 Tesla	Equal variances Assumed	0.015	0.904	0.857	24	0.400	0.0183	0.213	−0.0257	0.0623
	Equal variances not assumed			0.857	23.993	0.400	0.0183	0.213	−0.0257	0.0623
Velocity @ 1.4 Tesla	Equal variances Assumed	0.013	0.911	0.888	24	0.383	0.0195	0.0219	−0.0258	0.0647
	Equal variances not assumed			0.888	23.993	0.383	0.0195	0.0219	−0.0258	0.0647
Velocity @ 3.0 Tesla	Equal variances Assumed	0.009	0.924	1.113	24	0.277	0.0250	0.0225	−0.0214	0.0713
	Equal variances not assumed			1.113	23.993	0.277	0.0250	0.0225	−0.0214	0.0713

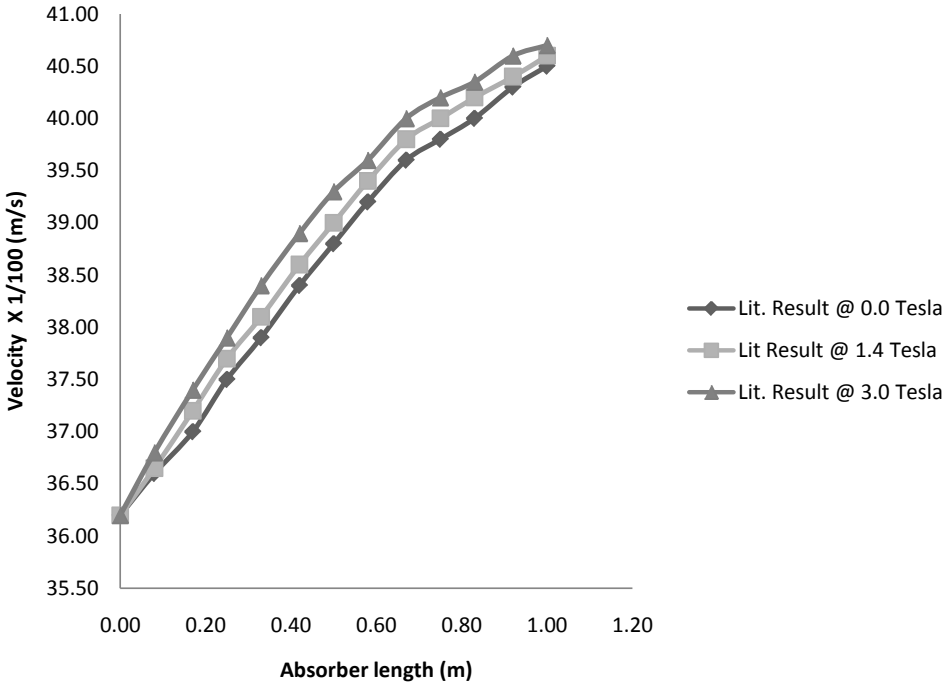

Figure 2. NH_3-H_2O Velocity Distribution in the film at 0.0, 1.4 and 3.0 Tesla for Xiao *et al*. [11].

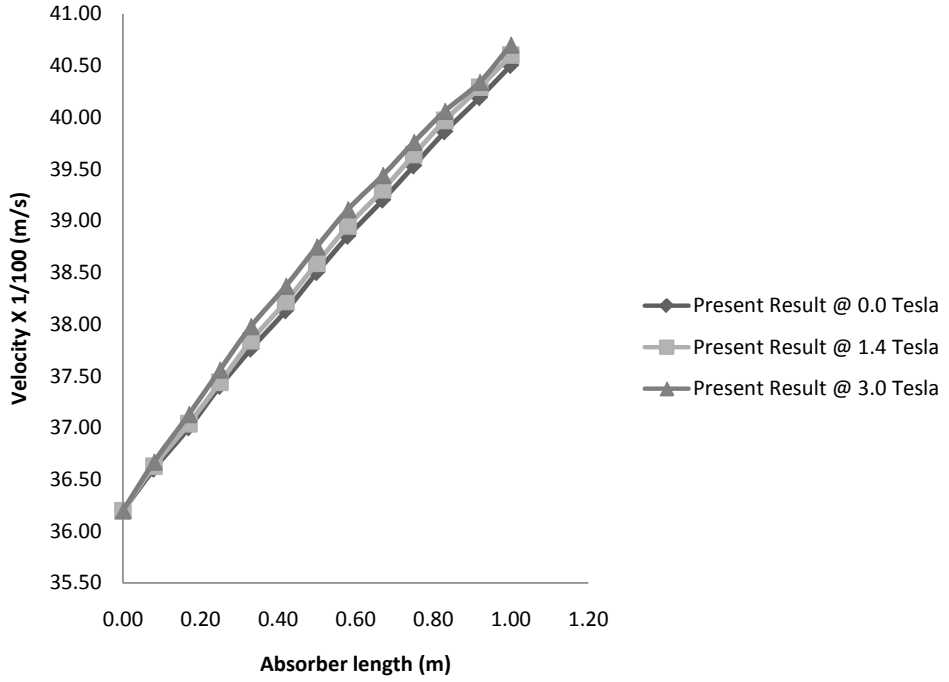

Figure 3. NH_3-H_2O Velocity Distribution in the film at 0.0, 1.4 and 3.0 Tesla for present work.

tiveities taken place at the interface which might constitute to the effect the magnetic intensity can have on the field. However, the overall results may suggest that the stronger the magnetic induction, the larger the average velocity.

Similarly, magnetic effect is not noticeable on the temperature distributions (**Figure 4** and **Figure 5**). It shows that the magnetic induction have no direct effect on the temperature. However, indirect effect might be possible as noticed in the velocity field. This is not surprising since continuous relationship exist between the velocity

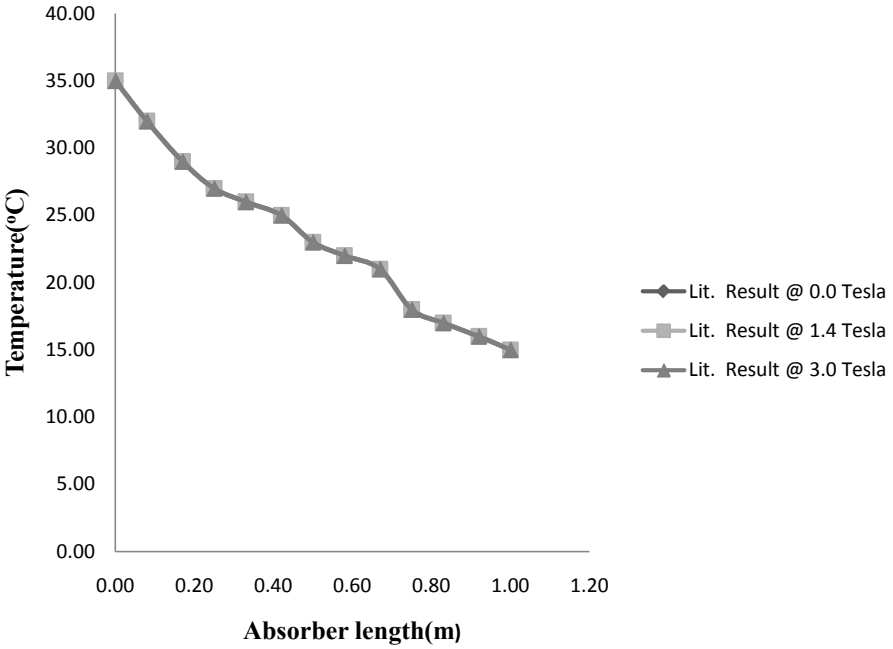

Figure 4. NH_3-H_2O Temperature Distribution in the film at 0.0, 1.4 and 3.0 Tesla for Xiao *et al*. [11].

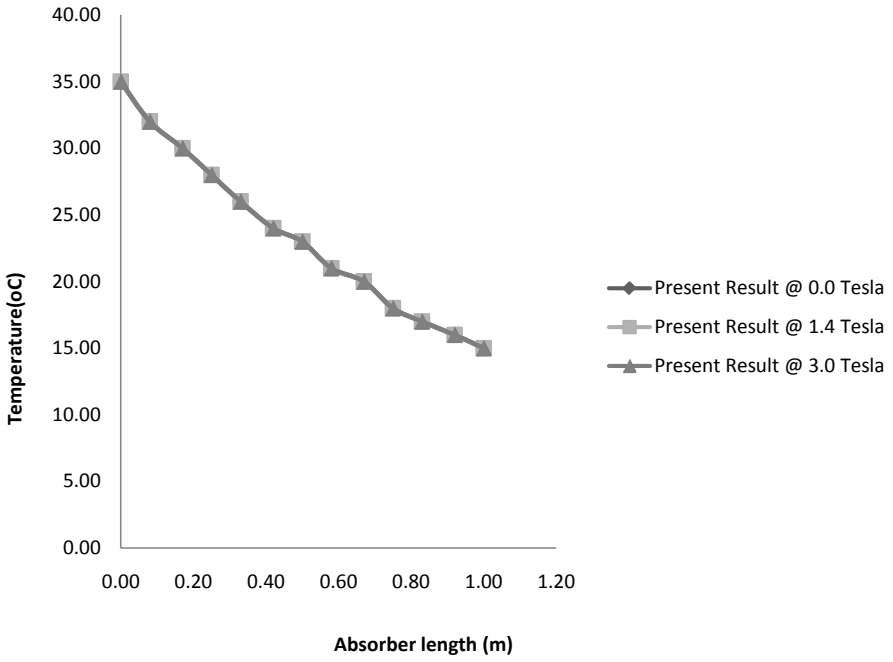

Figure 5. NH_3-H_2O Temperature Distribution in the film at 0.0, 1.4 and 3.0 Tesla for present work.

and temperature fields. The effect is likely to be stronger at larger Tesla.

Figure 6 and **Figure 7** show the concentration distributions in the film for Xiao *et al*. [11] and the present work respectively. While Xiao *et al*. [11] shows some level of departure from 0.0 Tesla especially at 3.0 Tesla, the level of departure in the present study is not significant in the film. However, it may be inferred from the distributions that application of magnetic induction does not changed the steady relationship that do exist among the parameters.

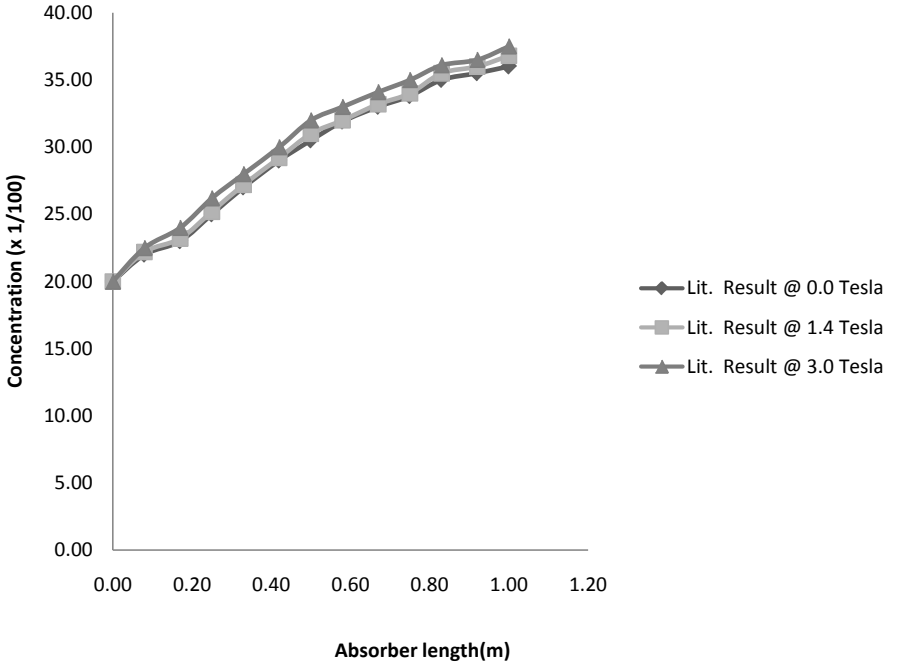

Figure 6. NH_3-H_2O Concentration Distribution in the film at 0.0, 1.4 and 3.0 Tesla for Xiao *et al*. [11].

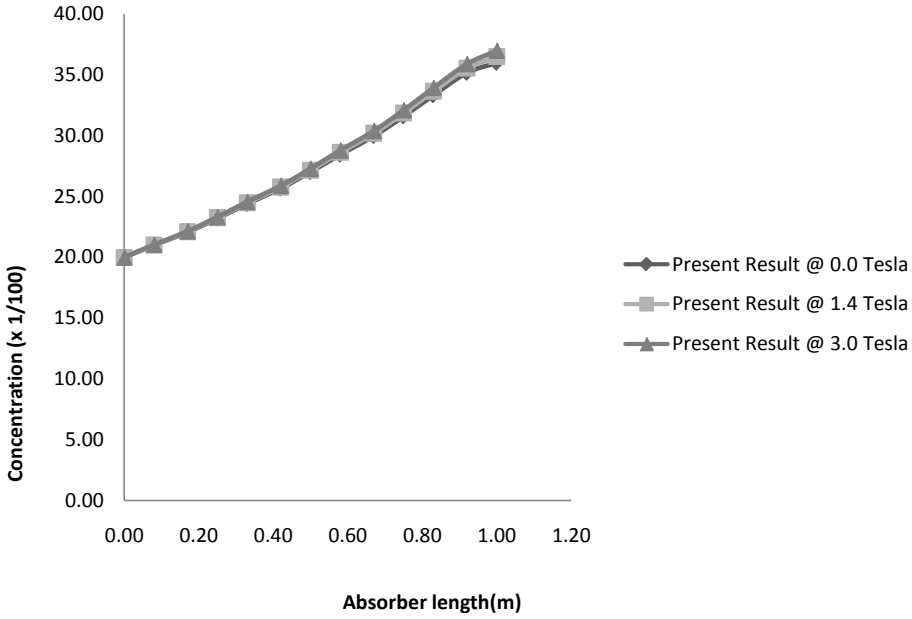

Figure 7. NH_3-H_2O Concentration Distribution in the film at 0.0, 1.4 and 3.0 Tesla for present work.

4.2. Coefficient of Performance (*COP*) for NH_3-Water Absorption Refrigeration

Coefficient of performance (*COP*) of an absorption refrigeration system is obtained from:

$$COP = \frac{\text{cooling capacity obtained at evaporator}}{\text{heat input for the generator} + \text{pump work output}}$$

or

$$COP = \frac{\text{concentration at the outlet}}{\text{concentration at the inlet}}$$

The work input for the pump is negligible relative to the heat input at the generator; therefore, the pump work is often neglected for the purposes of analysis.

From the result

At 0.0 Tesla, COP = 0 to 3 Tesla 518/0.2 × 100% = 175.9%

At 1.4 Tesla, COP = 0 to 3 Tesla 555/0.2 × 100% = 177.75%

At 3.0 Tesla, COP = 0 to 3 Tesla 590/0.2 × 100% = 179.5%

Increment at 1.4 Tesla relative to 0.0 Tesla = (179 − 177.75) % = 1.9%

Increment at 3.0 Tesla relative to 0.0 Tesla = (179.5 − 175.9) % = 3.6%

4.3. Results in the Direction of the Film Thickness (δ)

The velocity distribution across the film thickness direction at sections X = 0.25 m in three different magnetic induction intensities are shown in **Figure 8** and **Figure 9**. A dimensionless parameter of y/δ is used as the abscissa. It can be seen from **Figure 8** and **Figure 9** that the distributions remains constant until a certain value of y/δ is reached before started to increase with increase in the magnetic induction (β). This could be explained as follows: At the inlet section, absorption has just begun in an intense way and the film thickness is very thin, the absorption enhancement effect by magnetic field is obvious, turbulence in direction of thickness therefore are more intense due to the above mentioned reasons. Velocity variations along the thickness direction at the selected section have the tendency of increasing from absorber wall to the vapour-liquid interface as established. This indicates that the refrigerants vapour in the working fluid permeates towards the inner solution from the vapour-liquid interface. When the liquid film drops, the increase in velocity is slowed down. Thus the result establishes positive influence of the magnetic field enhancement on the working fluid.

5. Conclusion

The absorption process modeling of a smooth thin-liquid falling-film in ammonia-water absorption system in magnetic field enhancement medium has been undertaken. The developed mathematical model for the magnetic field enhancement of ammonia water absorption system was established. The model equations were developed from the continuity, momentum, energy, concentration or species and mass transport equations. The changes in physical properties of the working fluid in absorption system within the smooth thin-liquid film thickness along falling and across the film in the direction of its thickness were considered. Distributions of velocity, tempera-

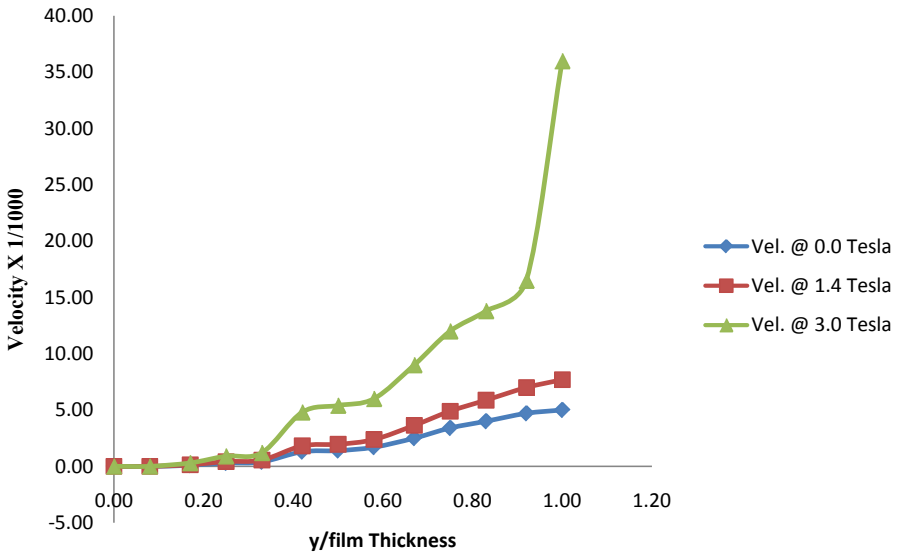

Figure 8. NH_3-H_2O velocity distribution in the direction of film thickness at X = 0.25 m for Xiao *et al.* [11].

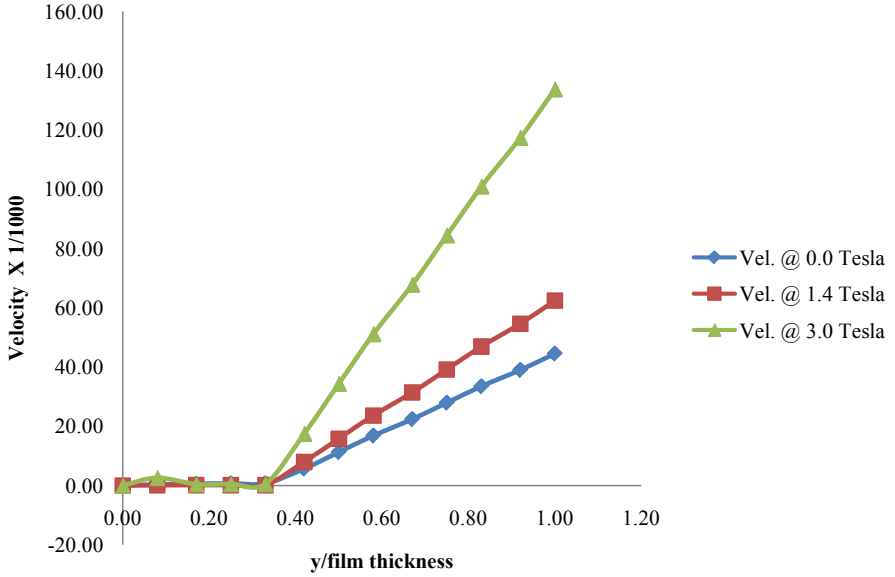

Figure 9. NH_3-H_2O velocity distribution in the direction of film thickness at X = 0.25 m for present work.

ture and concentration both in the direction of falling-film and across the film thickness with the magnetic field intensity in the range of 0 to 3 Tesla were obtained. The results obtained show that magnetic field improved the performance of ammonia-water falling film absorption, and the effect increases with increased in magnetic intensity. While the distributions of velocity showed significant changes in the presence of magnetic induction, the changes in temperature and concentration distributions are not significant. The results of the velocity across the film thickness revealed the positive influence of the magnetic field enhancement on the working fluid.

References

[1] Adaramola, M.S., Oyewola, O.M., Ohunakin, O.S. and Akinnawonu, O.O. (2014) Performance Evaluation of Wind Turbines for Energy Generation in Niger Delta, Nigeria. *Sustainable Energy Technologies and Assessments*, **6**, 75-85. http://dx.doi.org/10.1016/j.seta.2014.01.001

[2] Adaramola, M.S., Oyewola, O.M., Ohunakin, O.S. and Dinrifo, R.R. (2012) Techno-Economic Evaluation of Wind Energy in Southwest Nigeria. *Frontiers of Energy*, **6**, 366-378. http://dx.doi.org/10.1007/s11708-012-0205-y

[3] Ohunakin, O.S. (2010) Energy Utilization and Renewable Energy Sources in Nigeria. *Journal of Engineering and Applied Science*, **5**, 171-177. http://dx.doi.org/10.3923/jeasci.2010.171.177

[4] Ohunakin, O.S., Leramo, O.R., Abidakun, O.A., Odunfa, M.K. and Bafuwa, O.B. (2013) Energy and Cost Analysis of Cement Production Using the Wet and Dry Processes in Nigeria. *Energy and Power Engineering*, **5**, 537-550. http://dx.doi.org/10.4236/epe.2013.59059

[5] Yang, R. andWood, B.D. (1992) A Numerical Modeling of an Absorption Process on a Liquid Falling Film. *Solar Energy*, **48**, 195-198. http://dx.doi.org/10.1016/0038-092X(92)90138-Z

[6] Kimand, D.S. and Infante-Ferreira, C.A. (2008) Solar Refrigeration Options: A State of the Art Review. *International Journal of Refrigeration*, **31**, 3-15. http://dx.doi.org/10.1016/j.ijrefrig.2007.07.011

[7] Chen, J.H., Chang, H. and Chan, S.R. (2006) Simulation Study of a Hybrid Absorber-Heat Exchanger Using Hollow Fiber Membrane Module for the Ammonia-Water Absorption Cycle. *International Journal of Refrigeration*, **29**, 1043-1052. http://dx.doi.org/10.1016/j.ijrefrig.2006.02.002

[8] Yong, T.K., Hyun, J.K. and Kang, I.L. (2008) Heat and Mass Transfer Enhancement of Binary Nanofluids for H_2o/Libr Falling Absorption Process. *International Journal of Refrigeration*, **31**, 850-856. http://dx.doi.org/10.1016/j.ijrefrig.2006.02.002

[9] Niu, X., Du, K. and Du, S. (2007) Numerical Analysis of Falling Film Absorption with Ammonia-Water in Magnetic Field. *Applied Thermal Engineering*, **27**, 2059-2065. http://dx.doi.org/10.1016/j.applthermaleng.2006.12.001

[10] Wen-Long, C., Kouich, H., Ze-Shao, C., Atsushi, A., Peng, H. and Takao, K. (2004) Heat Transfer Enhancement by Additive in Vertical Falling Film Absorption of H_2O/LiBr. *Applied Thermal Engineering*, **24**, 281-298.

http://dx.doi.org/10.1016/j.applthermaleng.2003.08.013

[11] Xiao, F.N., Kai, D. and Xiao, F. (2010) Experimental Study on Ammonia-Water Falling Film Absorption in External Magnetic Fields. *International Journal of Refrigeration*, **30**, 1-9.

[12] Bird, E.B., Steward, W.E. and Light-foot, E.N. (1960) Transport Phenomena. Wiley, New York.

[13] Li, G.D. (1999) Contemporary Magnetism. University of Science and Technology, China Press Ltd.

[14] Andberg, G.W. (1982) Non-Isothermal Absorption of Gases into Falling Liquid Film. M.Sc. Thesis, University of Texas at Austin, Texas.

Nomenclature

μ	[kg/m·s^{-1}]	film dynamic viscosity
υ_o	[m·s^{-1}]	Mean velocity
α	[m^2/s]	thermal diffusivity
k	[W/mK]	Thermal conductivity of the fluid
ρ	[kg/m^3]	liquid density
D	[m^2/s]	species diffusivity
β	[K^{-1}]	cubic expansivity of fluid
T_w	[˚C]	dimensional wall temperature
T_{in}	[K]	inlet refrigerant temperature
C_{in}	[%]	initial absorbent concentration
C_{eq}	[%]	equilibrium absorbent concentration
g	[m·s-1^2]	Acceleration due to gravity
h_0	[m]	Mean film thickness
ν	[m^2/s]	kinematic viscosity of fluid
Ha	[kJ/kg]	heat of absorption
Pv	[mm·Hg]	absorbent vapour pressure

Appendix

1) Main Program

The flow charts are as shown in **Figures 10-12**. This main program utilizes two (2) different subroutines. These subroutines are written to execute various steps involved in applying the finite difference scheme. The problem data are introduced into the program in the "data block", where the input parameters can be easily modified to suit any case study. The main program, after generating the global matrix, calls subroutine "solution 1", before calling subroutine "solution 2". After calling a subroutine solution the results were finally "displayed".

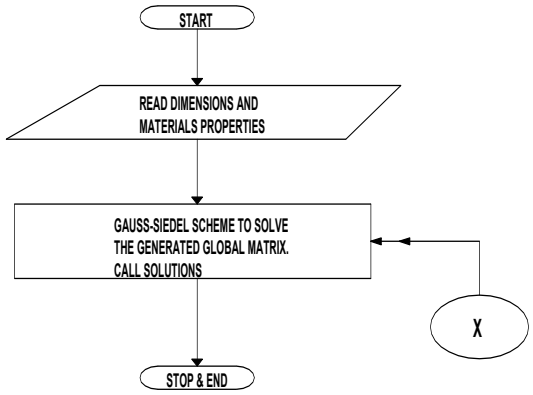

Figure 10. Main program flow chart.

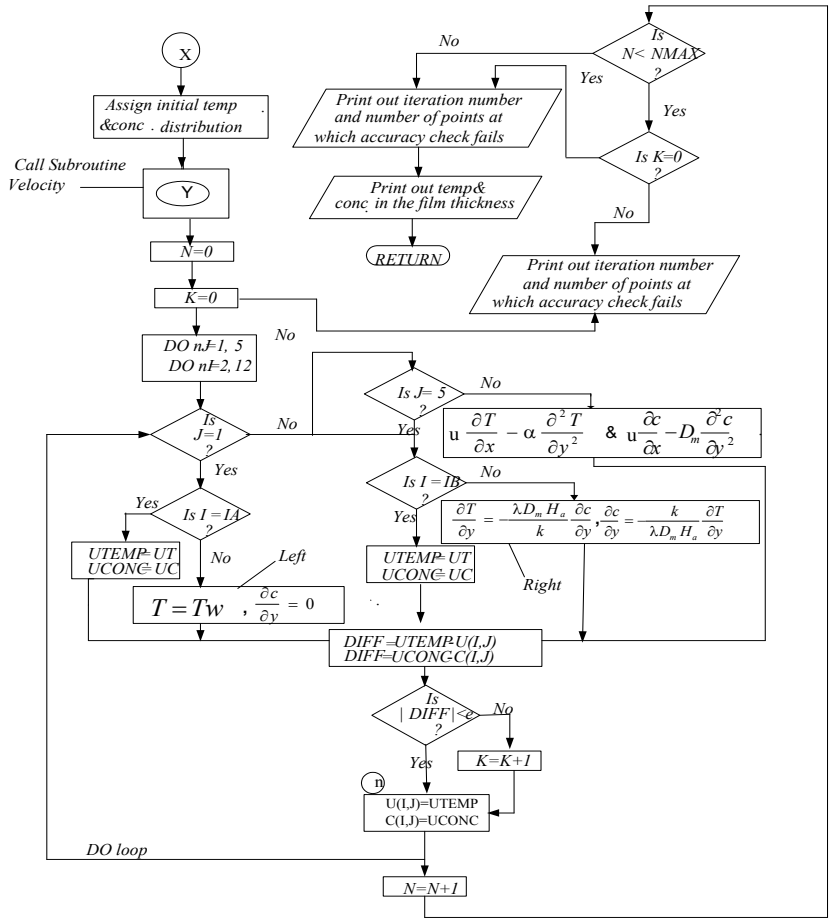

Figure 11. Subroutine solution flow chart.

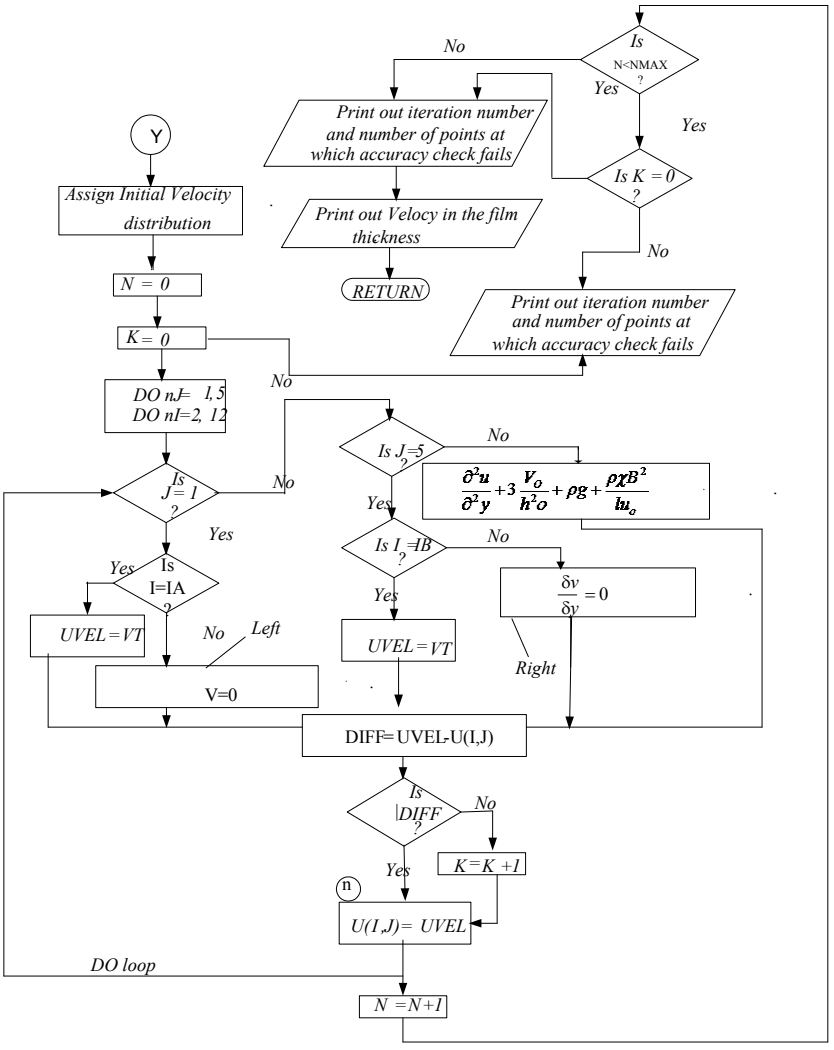

Figure 12. Model subroutine velocity flow chart.

2) Subroutines

These are sub-programs written to execute various steps involved in applying the finite difference method using Gaussian elimination scheme. They are called by the main program. Below are the subroutines employed to execute various steps in the main program

3) Solution 1 & Solution 2

These are the core sub-routines, they also perform similar functions. These subroutines perform their functions after the implementation of the boundary conditions in the global domain. Solution 1 generates the temperature profile of the domain, while solution 2 takes care of concentration profile within the domain.